Molecular and Histological Evidence Detailing Clinically Observed Skin Improvement Following Cryolipolysis

W. Grant Stevens, MD, FACS; Daniel J. Gould, MD, PhD; Linda D. Pham, PhD; and Joel N. Jimenez Lozano, PhD

Aesthetic Surgery Journal
2022, Vol 42(1) 56–67

DOI: 10.1093/asj/sjab226
www.aestheticsurgeryjournal.com
OXFORD UNIVERSITY PRESS

Abstract

Background: In addition to body contouring, there is anecdotal and clinical evidence of reduced laxity caused by skin tightening after cryolipolysis. However, it has not been established how cryolipolysis triggers dermal changes.

Objectives: The aim of this study was to investigate the fundamental mechanisms behind clinically observed dermal changes by molecular and immunohistochemistry (IHC) analytical methods.

Methods: This feasibility study involved 7 subjects who received cryolipolysis treatment. Tissue samples were harvested from 3 days to 5 weeks after treatment. RNA-sequencing examined differential gene expression of major collagens. RNA in situ hybridization (RNA-ISH) investigated the distribution of 1 of the gene markers for collagen type I (COL1A1). IHC for procollagen type I, heat shock protein 47 (HSP47), transforming growth factor β (TGF-β), and tropoelastin was performed and quantified.

Results: Gene expression analysis highlighted a gradual upregulation of collagen mRNA genes. RNA-ISH confirmed upregulation of COL1A1 mRNA and showed a homogeneous distribution through the dermis. IHC showed increases in protein expression. Quantification revealed a 3.62-fold increase of procollagen type I ($P < 0.0071$), a 2.91-fold increase of TGF-β ($P < 0.041$), a 1.54-fold increase of HSP47 ($P < 0.007$), and a 1.57-fold increase of tropoelastin ($P < 0.39$) compared with untreated areas.

Conclusions: This study revealed significant induction of molecular and protein markers of type I collagen, which supports neocollagenesis and may play an essential role in clinically relevant skin improvement. A dermal remodeling process driven by increased TGF-β and higher expression of HSP47 was observed. Overall, these data provide the first evidence of dermal remodeling and clarify the mechanism by which cryolipolysis may induce skin improvement.

Level of Evidence: 4

Editorial Decision date: April 29, 2021; online publish-ahead-of-print May 17, 2021.

Cryolipolysis is a well-known noninvasive fat reduction procedure that utilizes controlled cooling to target subcutaneous fat and induce adipocyte apoptosis. Numerous clinical studies have demonstrated the safety, efficacy, and tolerability of cryolipolysis for reducing fat in body areas including the abdomen, flank, upper arm, submental area, and thighs.[1-10]

Although the use of cryolipolysis to reduce subcutaneous fat is well-established, there have also been several anecdotal reports of improvements in skin over the

Dr Stevens is a clinical professor of surgery, University of Southern California, Los Angeles, CA, USA. Dr Gould is a plastic surgeon in private practice in Marina del Rey, CA, USA. Dr Pham is an associate director and Dr Jimenez Lozano is a scientist and senior manager at Allergan Aesthetics, an AbbVie affiliate, Pleasanton, CA, USA.

Corresponding Author:
Dr W. Grant Stevens, 4560 Admiralty Way, Suite 256, Marina del Rey, CA 90292, USA.
E-mail: drstevens@hotmail.com

Figure 1. A 51-year-old female patient (A, C) before treatment for back fat and (B, D) 6 months after 2 cryolipolysis cycles to the back. Figure courtesy of the International Society of Aesthetic Plastic Surgery.[15]

treated areas. This was first reported in the literature by Stevens, who coined the term "cryodermadstringo" to highlight overall changes to the skin following cryolipolysis and then followed up with additional reviews of specific body areas incorporating independent physician assessments and patient surveys that quantified improvements in skin laxity, skin texture, and cellulite.[11,12] A study of submental area cryolipolysis showed not just fat reduction but quantified skin tightening as well.[13] The manufacturer of the cryolipolysis system used in the submental fat reduction study subsequently obtained FDA clearance to use the system to improve the appearance of lax tissue after submental treatment.[14] Figures 1 to 4 show clinical photographs of cryolipolysis patients.[6,11,15] Although the patients underwent the procedure for noninvasive fat reduction, these clinical before-and-after photographs also illustrate skin improvement in the treated areas. The laxity seen in the back, buttocks, abdomen, and flanks appears reduced in the posttreatment photographs, which show fewer horizontal creases and textural irregularities in the overlying dermal tissue.

Some clinicians have described the perceived skin improvement as skin tightening or skin retraction. However, fundamental evidence of changes to the skin and an exploration of the mechanism of action by which cryolipolysis induces alterations to skin overlying the treatment area have not previously been reported. A short review of the effects of laser-, light-, and radiofrequency-based technologies on skin laxity was provided by Sadick.[16] Noninvasive device studies have shown skin tightening from energy-based devices that produce heating in the tissue with radiofrequency, microfocused ultrasound, and laser modalities.[17-22]

Molecular and immunohistochemistry (IHC) methods have been used to assess the mechanisms underlying skin changes following laser therapy[23,24] and radiofrequency treatment.[25,26] Most of these works were focused on

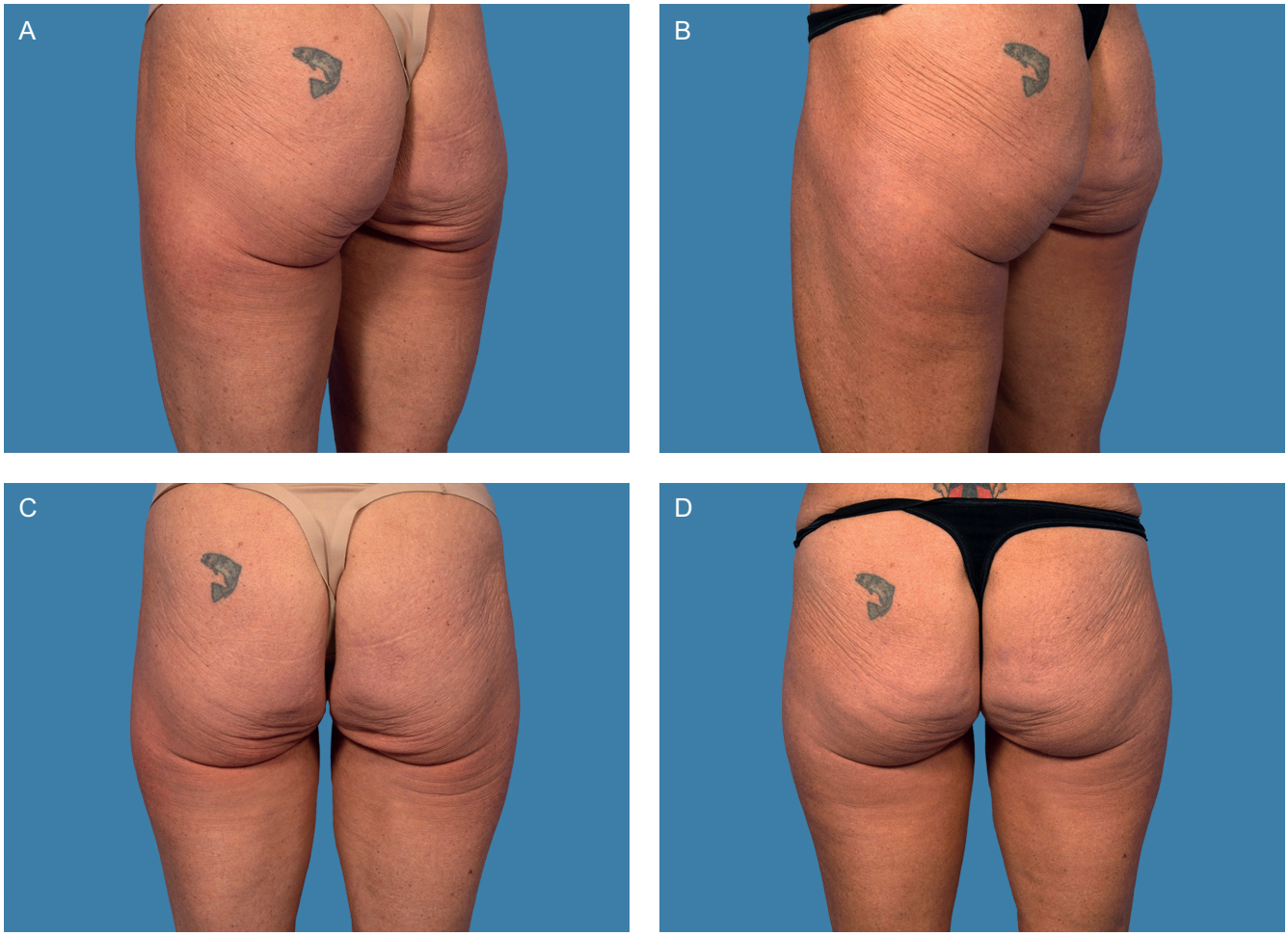

Figure 2. A 57-year-old female patient (A, C) before treatment of "banana rolls" under her buttocks and (B, D) 5 months after 2 cryolipolysis cycles on each side.By permission of Oxford University Press.[6]

finding changes in collagen and elastin proteins and their gene expression, along with other important markers of the skin extracellular matrix, ie, cytokines and growth factors.

The motivation for the current study was to better understand the clinical observations of skin improvement after cryolipolysis by investigating dermal changes by both molecular and IHC analytical methods.

METHODS

This was a multicenter, prospective, open-label, nonrandomized feasibility study. The protocol was approved by an IRB (Salus IRB, Austin, TX). Eligible subjects were male or female, at least 18 years of age, with a scheduled surgical excision of abdominal fat and skin. All subjects provided written informed consent prior to participating in the study.

Exclusion criteria included previous surgical procedures such as liposuction or noninvasive fat reduction in or near the treatment area in the past 6 months, a known history of cryoglobulinemia, cold urticaria, cold agglutinin disease, paroxysmal cold hemoglobinuria, Raynaud's disease, bleeding disorders or concurrent medications that could increase the risk of bruising, and dermatologic conditions such as excessive skin laxity or scars that may interfere with the treatment or evaluation.

Study subjects were treated on the abdomen with a cryolipolysis system (CoolSculpting; Zeltiq Aesthetics, Pleasanton, CA), applying 1 cycle (–11°C for 35 minutes) per treatment site delivered by a cooled cup vacuum applicator (CoolAdvantage).

Cryolipolysis was delivered to one side of the lower abdomen; the contralateral side served as the untreated control. A protective gel pad (CoolAdhesive) was applied to the skin and suction was initiated. With the applicator secured to the treatment area, the subject reclined throughout the cryolipolysis procedure. At the end of the treatment cycle, the applicator was removed, and a manual massage of

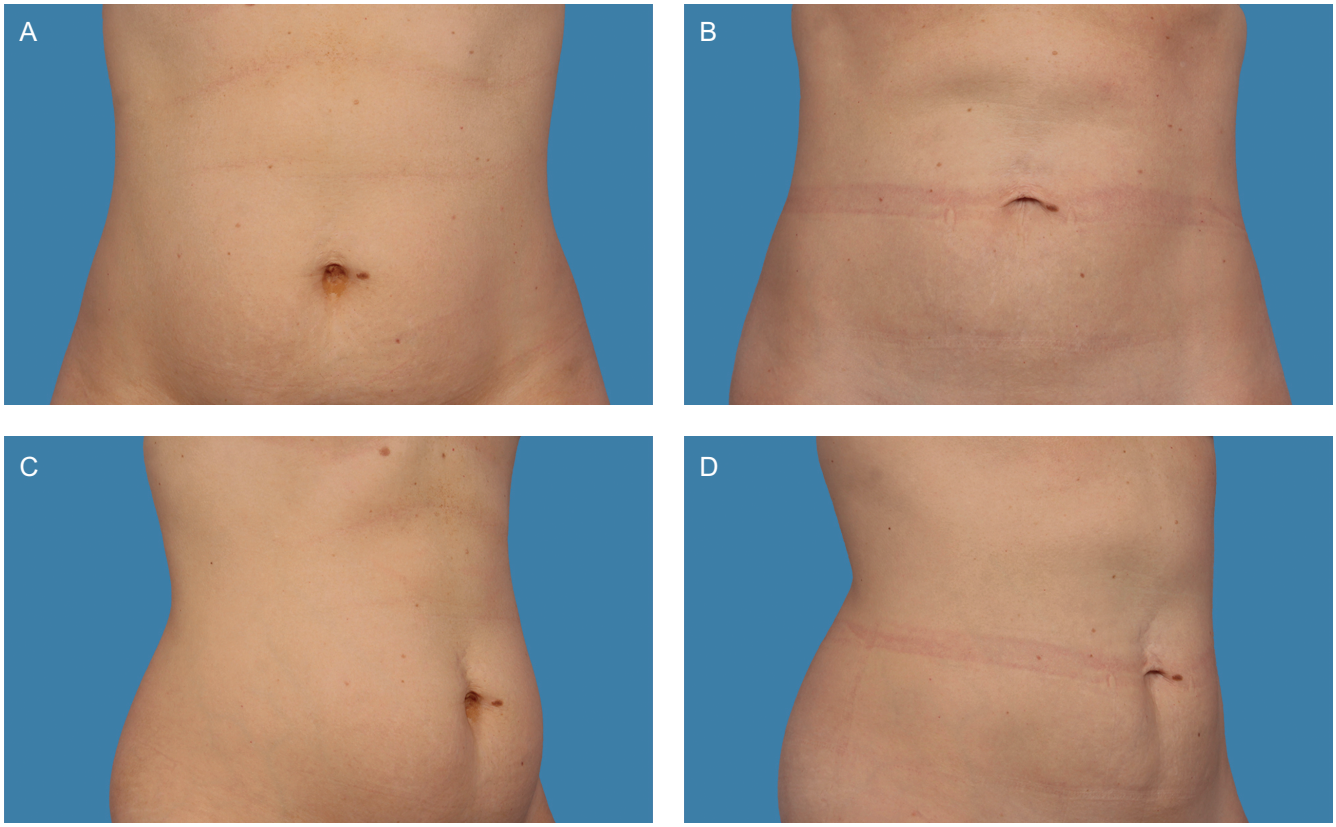

Figure 3. A 38-year-old female received 2 cryolipolysis cycles to the lower abdomen and 2 cycles to the upper abdomen: (A, C) pretreatment; (B, D) 4 months posttreatment. By permission of Oxford University Press.[11]

the treatment area was performed for 2 minutes. Safety was monitored by documentation of any adverse events throughout the study, as was clinical assessment of the treatment site.

One treated and 1 untreated control sample, approximately 1 inch × 1 inch × 1 inch (25 mm × 25 mm × 25 mm) through the skin and fat, were taken from the whole tissue abdominoplasty sample of each study subject. Harvested tissue was immediately placed in fixative after surgery and later processed for gene expression and IHC analysis, as described below.

RNA-Sequencing

Total cellular RNA was isolated from skin tissue biopsies with the RNeasy Lipid Tissue Mini Kit (Qiagen, Hilden, Germany) following the manufacturer's recommended instructions. In brief, approximately 100 mg of starting tissue was lysed and extracted with a combination of QIAzol Lysis Reagent and chloroform. RNA-containing lysates were adjusted to optimal silica membrane–binding conditions and spun through a membrane-containing column. Bound RNA was washed several times to remove any residual contaminants and treated with DNase to prevent contaminant DNA carryover. The purified RNA was eluted from the membrane with nuclease-free water and subjected to the following analyses. RNA quantity and quality were determined by Nanodrop UV spectrophotometry (Thermo Fisher, Waltham, MA) and Bioanalyzer analysis (Agilent, Santa Clara, CA), respectively. RNA quality was determined with the RNA 6000 Nano Kit (Agilent) on the Bioanalyzer. All samples resulted in adequate RNA quality-control results for sequencing.

One microgram of isolated RNA was subjected to library preparation with the TruSeq stranded mRNA library preparation kit (Illumina, San Diego, CA) as per the manufacturer's instructions. Briefly, mRNA was selected from the total RNA pool by serial binding to oligo(dT) magnetic beads. The isolated mRNA was fragmented and used as a template to generate cDNA. The resultant cDNA was subject to 3′ adenylation, adaptor ligation, and subsequent amplification via polymerase chain reaction. The amplified DNA libraries were cleaned-up and concentrated via Solid Phase Reversible Immobilization beads (Beckman Coulter Life Sciences, Indianapolis, IN). The final DNA libraries were analyzed for quality and quantity with the Bioanalyzer (High Sensitivity DNA Analysis Kit; Agilent).

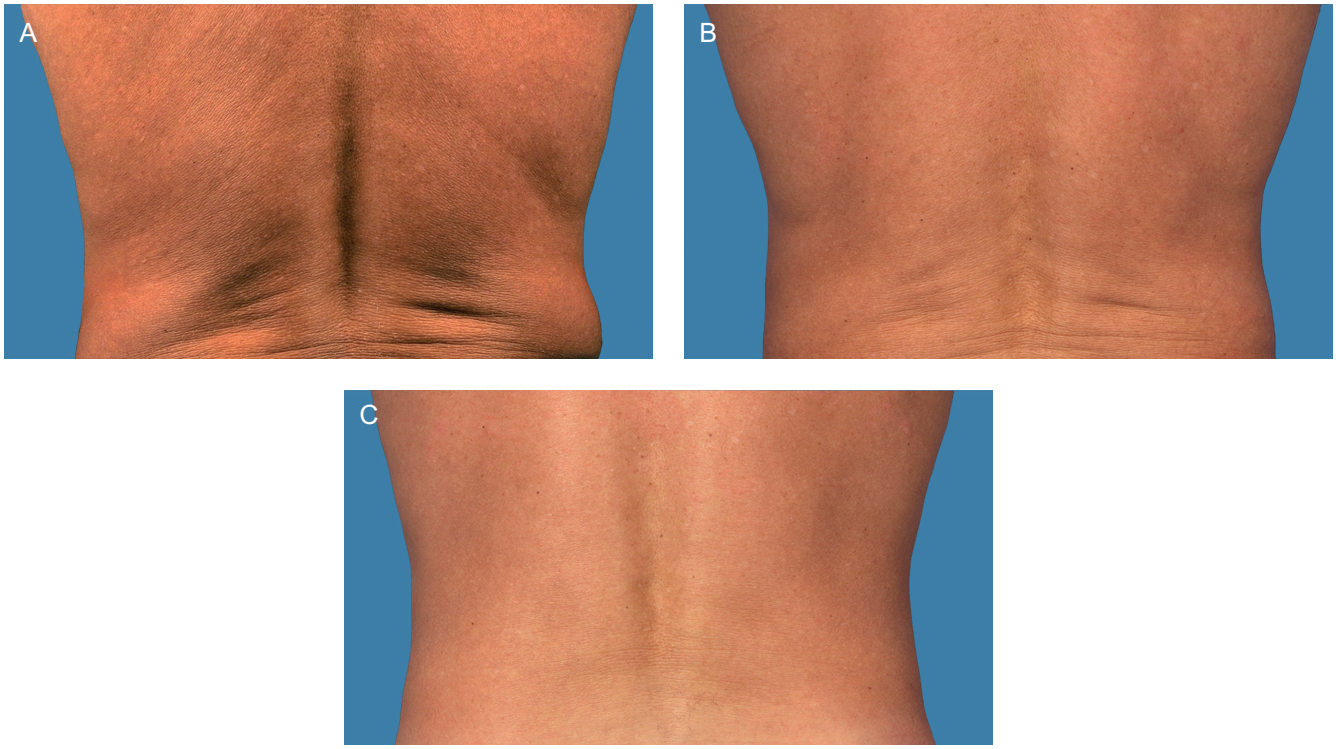

Figure 4. (A) A 58-year-old male patient prior to cryolipolysis treatment of the flanks. (B) One year after the first treatment and (C) an additional 1 year after the second treatment. No weight change since baseline.By permission of Oxford University Press.[6]

The mRNA libraries were sequenced on 2 NextSeq (Illumina) runs to a depth of 20 million 75-bp paired-end reads. Both NextSeq sequencing runs had percentage ≥Q30 quality scores of ≥89%. Sequence files from the 2 NextSeq runs were used for RNA-sequencing (RNA-seq) analysis according to the "Tuxedo protocol" pipeline, which reports differential gene and transcript expression.[27] Heat maps were created with the clustergram function in Matlab 14 (Mathworks, Inc., Natick, MA) of selected differentially expressed genes.

RNA In Situ Hybridization

RNA in situ hybridization (RNA-ISH) assay was performed according to the Invitrogen ViewRNA ISH Tissue Assay protocol (Invitrogen, Carlsbad, CA) with the following optimized pretreatment conditions: heat pretreatment for 10 minutes at 90 to 95°C; protease digestion at 1:100 dilution for 10 minutes at 40°C; COL1A1, a human collagen type I probe (Thermo Fisher; #VA6-18298) was used for the assay. Hybridization for human COL1A1 was performed for 2 hours at 40°C.

Human glyceraldehyde-3-phosphate dehydrogenase (GAPDH) (Thermo Fisher; #VA6-10337) + dihydrodipicolinate reductase (dapB) (Thermo Fisher; #VF1-11712) probes were used for the 2-plex assay control. Hybridization was performed as follows: human COL1A1 for 2 hours at 40°C and human GAPDH + *Bacillus subtilis* dapB for 2 hours at 40°C.

IHC

Tropoelastin IHC was performed with a Leica Bond automated immunostainer (Leica Biosystems, Buffalo Grove, IL) and a rabbit anti-tropoelastin antibody (ab21600; Abcam, Cambridge, MA) at 1:1000 dilution. Tissue samples were stained alongside a no-primary negative control and a human skin positive control. Heat-induced antigen retrieval was performed with Leica Bond Epitope Retrieval Buffer 1 (citrate buffer, pH 6.0) for 20 minutes. Nonspecific antibody binding was blocked with Novolink Protein Block for 10 minutes. Primary antibody was applied for 20 minutes. Anti-rabbit poly-HRP-IgG antibody or Novolink Polymer (Leica; catalog #RE7280-CE, lot #6058461) was applied for 10 minutes. Endogenous peroxidase was blocked with Novolink Peroxide Block (Leica; catalog #RE7280-CE, lot #6058461) for 10 minutes. Anti-tropoelastin antibody was detected and visualized with 3′,3-diaminobenzidine (DAB; brown). A hematoxylin nuclear counterstain (blue) was applied.

Procollagen type I IHC was performed with a Leica Bond automated immunostainer and a rabbit anti-procollagen

I antibody (MilliporeSigma, Burlington, MA; #ABT257) at 1:250 dilution. Samples were stained alongside a no-primary negative control and a human skin positive control. Heat-induced antigen retrieval was performed with Leica Bond Epitope Retrieval Buffer 2 (EDTA buffer, pH 9.0) for 10 minutes. Nonspecific antibody binding was blocked with Novolink Protein Block for 10 minutes. Primary antibody was applied for 15 minutes. Anti-rabbit poly-HRP-IgG antibody or Novolink Polymer (Leica; catalog #RE7280-CE, lot #6058461) was applied for 8 minutes. Endogenous peroxidase was blocked with Novolink Peroxide Block (Leica; catalog #RE7280-CE, lot #6058461) for 10 minutes. Anti-procollagen I antibody was detected and visualized with DAB (brown). A hematoxylin nuclear counterstain (blue) was applied.

Transforming growth factor β (TGF-β) IHC was performed with a Leica Bond automated immunostainer and a mouse anti-TGF-β1 antibody (Santa Cruz Biotechnology, Dallas, TX; #sc-130348) at 1:50 dilution. Samples were stained alongside a no-primary negative control and a human placenta positive control. Heat-induced antigen retrieval was performed with Leica Bond Epitope Retrieval Buffer 2 (EDTA solution, pH 9.0) for 20 minutes. Nonspecific background was blocked with Novolink Protein Block for 10 minutes. Slides were incubated with primary antibody for 60 minutes. Rabbit anti-mouse IgG antibody was applied for 30 minutes. Anti-rabbit poly-HRP-IgG antibody or Novolink Polymer (Leica; catalog #RE7280-CE, lot #6058461) was applied for 15 minutes. Endogenous peroxidase was blocked with Novolink Peroxide Block (Leica; catalog #RE7280-CE, lot #6058461) for 10 minutes. Anti-TGF-β1 antibody was detected and visualized with DAB (brown). A hematoxylin nuclear counterstain (blue) was applied.

Heat shock protein 47 (HSP47) immunofluorescence staining was performed with the Leica Bond auto-immunostainer on samples at 1:250 dilution with a mouse-host anti-HSP47 antibody (Santa Cruz Biotechnology; catalog #sc-5293, lot #I2118). Samples were stained alongside a no-primary negative control and a human placenta positive control. Immunostaining was completed on the Leica Bond auto-immunostainer. Slides were dewaxed and antigen retrieval was performed with Leica Bond Epitope Retrieval Buffer 2 (EDTA solution, pH 9.0) for 20 minutes. Nonspecific background was blocked with Novolink Protein Block for 20 minutes. Staining was performed sequentially with a primary incubation of 2 hours, followed by secondary antibody incubation with AlexaFluor 647 donkey anti-mouse IgG (Invitrogen; #A31571) secondary antibody at 1:200 for 60 minutes. Slides were mounted with 4′,6-diamidino-2-phenylindole in Fluorogel II for nuclear visualization.

Table 1. Subjects, Posttreatment Time Points, and Sample Availability for Specific Analysis

Subject ID	Posttreatment time points (days)	RNA-seq	RNA-ISH	IHC
BAC-016	23	NA	Y	Y
BAC-017	9	NA	Y	Y
BAC-018	11	NA	NA	Y
OKA-034	3 31	Y (3 days)	NA	Y
OKA-035	3 17	Y (3 days)	NA	Y
	38			
OKA-037	10	Y	NA	Y
	24			
OKA-038	10	Y	NA	Y
	24			

Because of study limitations not all study subjects were sampled by all available analytical methods. IHC, immunohistochemistry; NA, not available; RNA-ISH, RNA in situ hybridization; RNA-seq, RNA sequencing.

Imaging and Quantification

Whole slide images were generated under bright-field or fluorescence illumination with a digital slide scanner (Pannoramic SCAN; 3DHistech, Budapest, Hungary). Image analysis data were generated by automated analysis of whole slide images with an integrated whole slide image management and automated image analysis workflow (ImageDx; Reveal Biosciences, San Diego, CA).

To quantify changes in procollagen type I, HSP47, TGF-β, and tropoelastin, digital images were processed with specialized software to automatically identify tissue, segment the regions of interest, classify the areas stained by the biomarker, and then quantify the segmented regions for biomarker positivity. This digital analysis permitted quantification of IHC and immunofluorescence stained slides for treated and untreated samples. Statistical data analysis was performed with a standard 2-tailed paired *t* test for means.

RESULTS

All 7 enrolled subjects completed the study between April 2018 and January 2019. All subjects were female with an average age of 42.5 years (range, 31-66 years) and an average BMI of 30.3 kg/m^2 (range, 26.9-34.0 kg/m^2). In order to study multiple posttreatment time points, some subjects had multiple treatment visits with a single

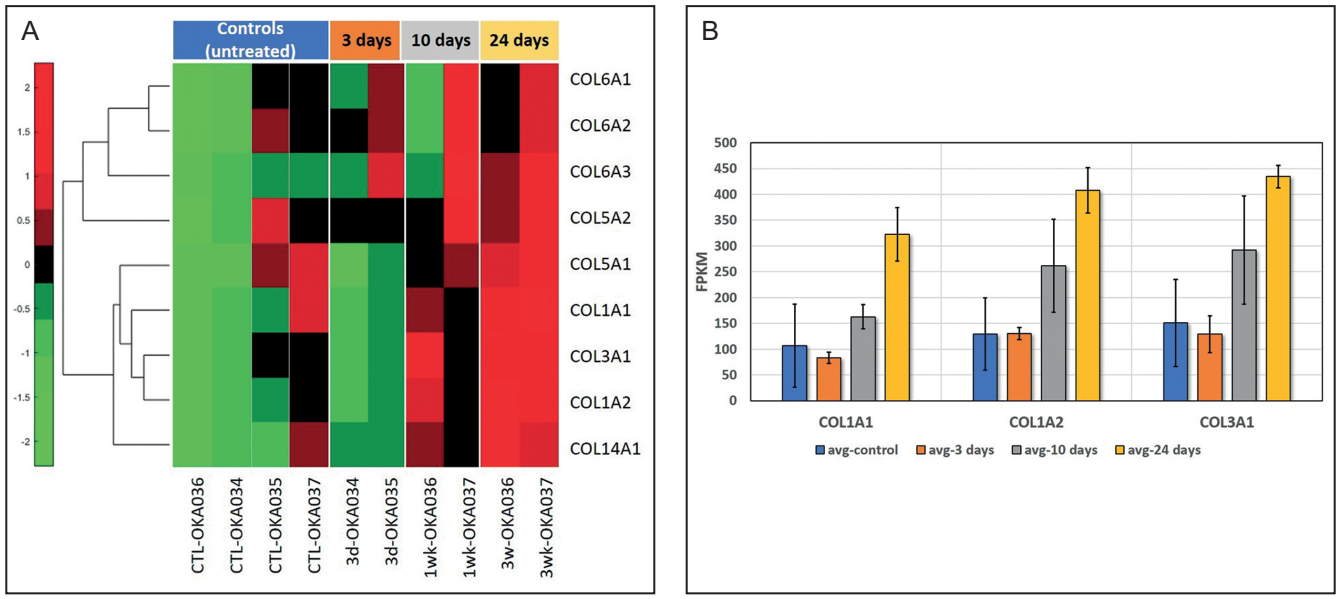

Figure 5. RNA-sequencing analysis of major collagens in the skin after cryolipolysis treatment. (A) Heat map shows an upregulation of collagen mRNA genes after treatment compared with the untreated samples; green represents upregulation and red downregulation. (B) Inset analysis of main dermal collagen type I and III mRNA genes: COL1A1, COL1A2, and COL3A1 are averaged for 3-, 10-, and 24-day time points. Data for FPKM vs averaged posttreatment time point. Bars show standard deviations. FPKM, fragments per kilobase of transcript per million mapped reads.

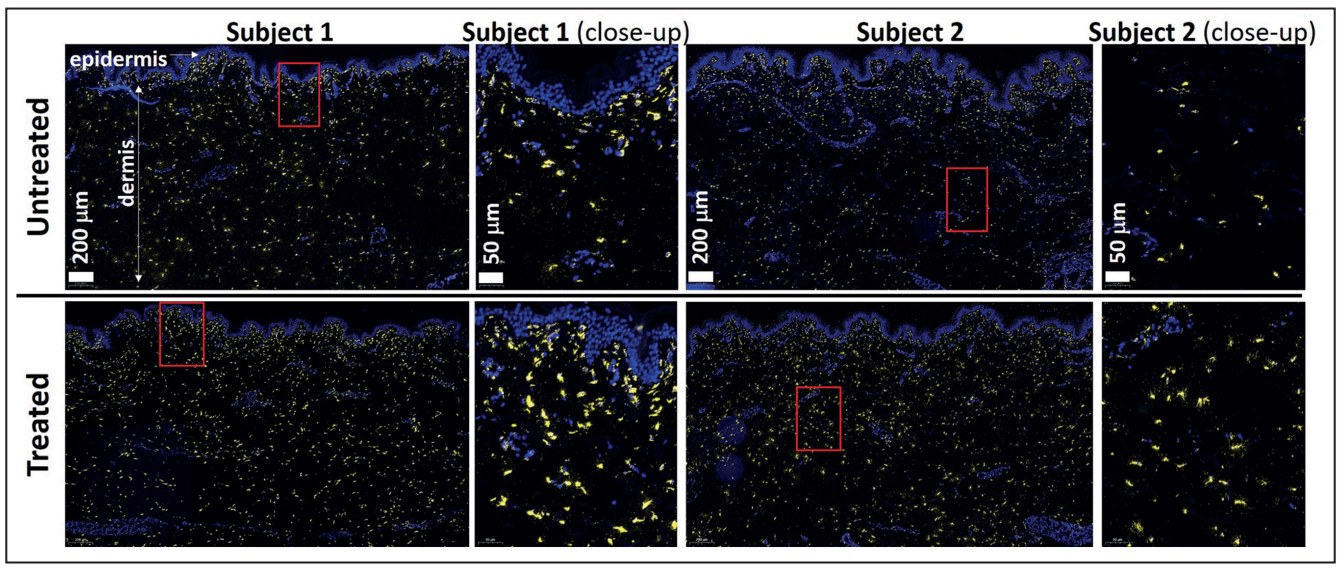

Figure 6. Representative samples of untreated (top row) and treated (bottom row) human skin samples analyzed by RNA in situ hybridization for the COL1A1 gene. Staining of COL1A1 is shown in yellow and nuclear stain in blue. Close-up views of the papillary and reticular dermis are shown. COL1A1 RNA in situ hybridization confirmed gene expression data and COL1A1 was found to be homogeneously distributed throughout the dermis in treated samples.

cycle per site as shown in Table 1. Because the dermal response timeline after cryolipolysis was unknown, the later posttreatment time points were spaced to approximately 3 weeks on average across all subjects.

Tissue samples were selected for either IHC, RNA-seq, and/or RNA-ISH such that sufficient tissue volume was collected for the proper processing according to the methods described herein and summarized in Table 1. Six samples

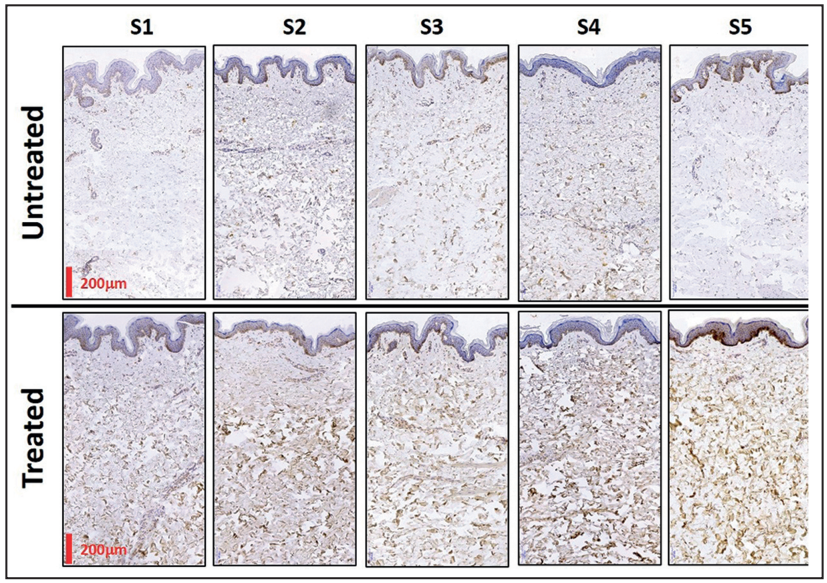

Figure 7. Representative samples of untreated (top row) and treated (bottom row) human skin from five subjects analyzed by immunohistochemistry for procollagen type I. Cryolipolysis-treated samples showed increased immunostaining for dermal procollagen throughout the dermis.

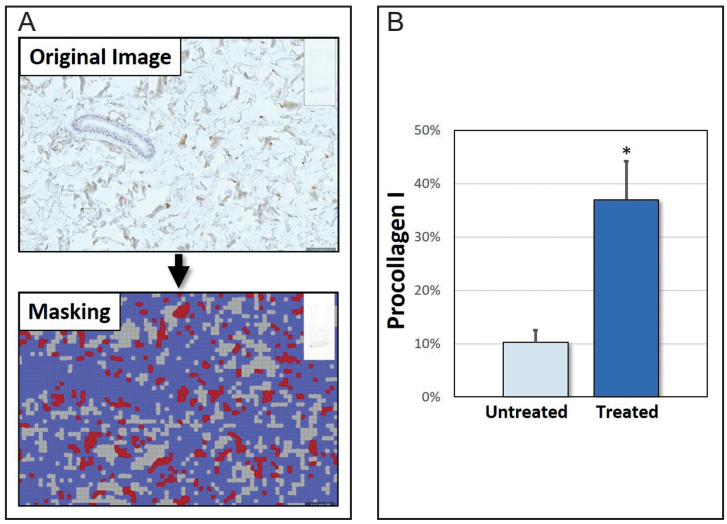

Figure 8. (A) Image analysis of the dermal procollagen and masking of positive (red pixels) and negative (blue pixels) marker-stained areas. (B) Quantification data of dermal procollagen type I in treated and untreated samples (*$P < 0.007$). Data for N = 11 samples, at a mean of 20.72 days posttreatment. Bars indicate standard errors of the mean.

and their untreated controls were available for RNA-seq. Similarly, treated and untreated samples from 2 subjects were available for RNA-ISH. All samples from subjects were available for IHC. Quantified IHC samples (N = 11) were obtained an average of 20.72 days posttreatment (excluding the 3-day samples used for RNA-seq only). There were no reported device- and/or procedure-related adverse events.

Figure 5 shows RNA-seq analysis of major skin collagens (in rows COL1A1, COL1A2, COL3A1, COL5A1, COL5A2, COL6A1, COL6A2, COL6A3, and COL14A1) in untreated controls and at 3, 10, and 24 days (columns) following cryolipolysis treatment. The heat map representation shows upregulation of these main dermal collagen genes following treatment. The inset magnification of the gene expression analysis for COL1A1, COL1A2, and COL3A1, which

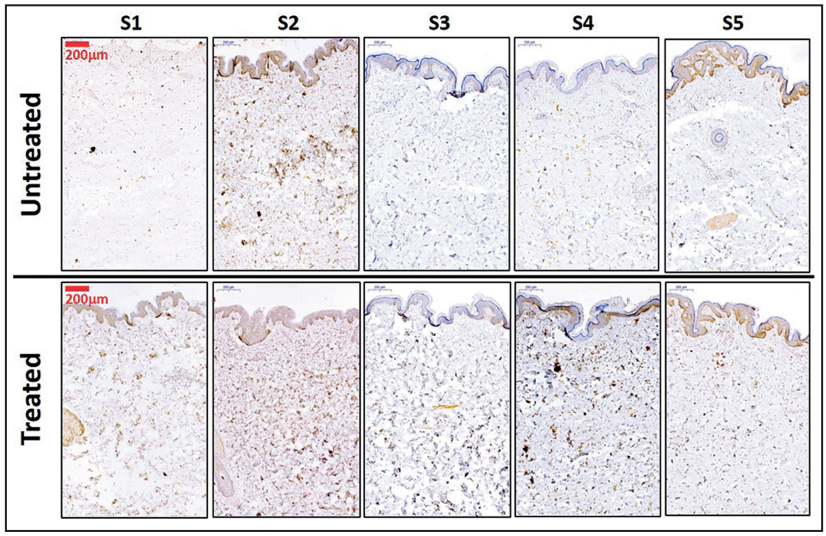

Figure 9. Representative samples of untreated (top row) and treated (bottom row) human skin from 5 subjects analyzed by immunohistochemistry for transforming growth factor β. Cryolipolysis-treated samples showed increased immunostaining for dermal transforming growth factor β throughout the dermis.

are the collagens that mainly contribute to the strength and stiffness to the skin, demonstrates a steady upregulation of these collagens at all 3 time points examined posttreatment.

RNA-ISH analysis of COL1A1 is shown for untreated and treated samples from 2 representative subjects in Figure 6. COL1A1 gene expression is shown in yellow fluorescence, whereas nuclear staining is shown in blue fluorescence. As shown in magnified inset views, in the papillary and reticular dermis an increase in yellow staining in the treated vs untreated samples demonstrates increased COL1A1 gene expression throughout the dermal layer following cryolipolysis treatment.

IHC-stained samples for procollagen type I are shown for 5 representative untreated and treated samples in Figure 7. Procollagen type I positivity is shown by brown stain. All treated samples showed increased staining throughout the dermal layer when compared with their untreated control (Figure 7). Procollagen type I was quantified as described in the Methods section.

In summary, image analysis of the original tissue slide was used for automated identification of tissue (removing voids and optical artifacts) and segmentation of regions of interest, then positive and negative marker areas were pixel masked (ie, red as positive, blue as negative; Figure 8A); and finally, the positive percentage was calculated from the positive procollagen area divided by the total area analyzed for each sample (Figure 8B). The increase in dermal procollagen type I in untreated vs treated samples was measured to be 3.62-fold; this change was statistically significant ($P < 0.007$) (Figure 8B).

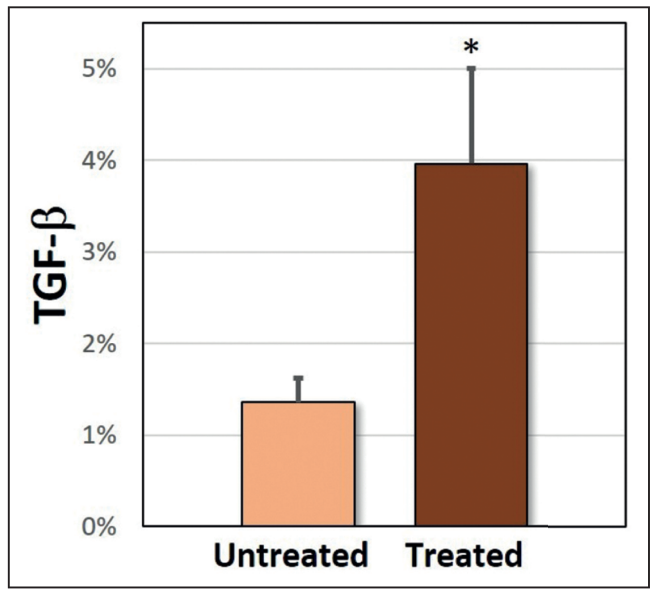

Figure 10. Quantification of dermal transforming growth factor β in treated and untreated samples (*$P < 0.041$). Subject data for N = 11 samples, at a mean of 20.72 days posttreatment. Bars indicate standard errors of the mean.

IHC-stained samples for TGF-β are shown for 5 representative untreated and treated subject samples in Figure 9; TGF-β positivity is shown by brown stain. All treated samples showed increased staining throughout the dermal layer vs the untreated sample (Figure 9). The dermal TGF-β was quantified by similar analytical

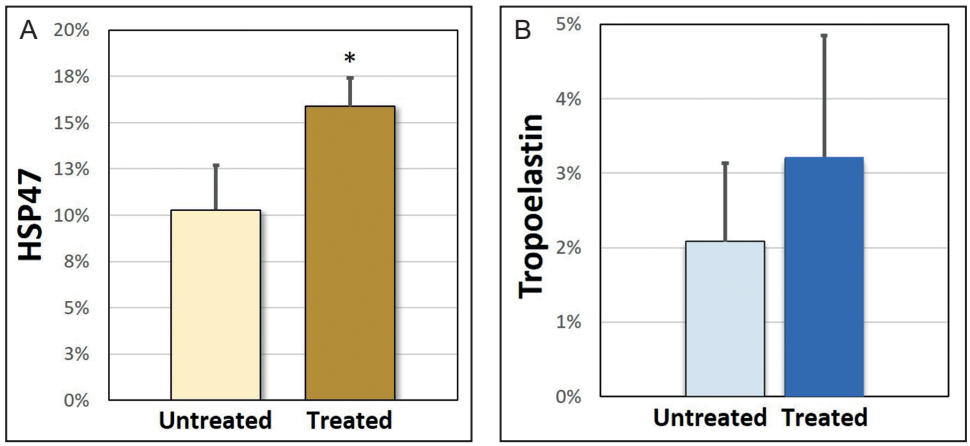

Figure 11. (A) Quantification of dermal heat shock protein 47 in treated and untreated samples (*$P < 0.007$). (B) Quantification of dermal tropoelastin in treated and untreated samples ($P < 0.39$). Subject data for N = 11 samples, at a mean of 20.72 days posttreatment. Bars indicate standard errors of the mean.

methods and found to increase 2.91-fold; this change was statistically significant ($P < 0.041$) (Figure 10).

Similarly, IHC-stained samples for HSP47 and tropoelastin were analyzed, and treated samples showed increased staining throughout the dermal layer vs their untreated control. The increases in dermal HSP47 and tropoelastin were quantified by similar analytical methods, as shown in Figure 11: HSP47 showed a statistically significant ($P < 0.007$) 1.54-fold increase; tropoelastin increased 1.57-fold although this was not statistically significant.

DISCUSSION

Although clinical observations of skin improvement with cryolipolysis have been previously reported in the literature,[11,12] the mechanism by which the change occurs has not previously been elucidated. This investigation is the first to show molecular and immunohistochemical evidence of dermal remodeling following cryolipolysis treatment. During cryolipolysis treatment, the skin transitions from body temperature to a supercooled unfrozen state across the dermal layer for the duration of the treatment cycle before rewarming to its initial state. To the best of our knowledge, subjecting skin to these specific conditions has not been studied in cryotherapy, cryobiology, or related medical research. Thus, the mechanisms by which dermal remodeling could occur after cryolipolysis are theoretical at best.

Previously, it was hypothesized that the "improved appearance in the skin may not actually be skin tightening but perhaps dermal thickening, resulting in an improved appearance to thin, crepey skin. The change in skin firmness may be the result of stimulated collagen production, new elastin formation, fibrosis, or tissue compaction."[11] The essential role of dermal fibroblasts in the expression of extracellular matrix markers such as collagen and elastin is well accepted.[28]

The results of the current study are limited by the small sample size but suggest that neocollagenesis plays a key role in dermal remodeling following cryolipolysis treatment. Future work should be carried out on a larger study subject population with randomized bilateral treated and untreated areas. Collagen data were taken from RNA-seq for analysis. Gene expression analysis demonstrated that cryolipolysis-treated skin samples had a gradual upregulation of collagen mRNA genes. The upregulation was confirmed by RNA-ISH analysis of COL1A1 mRNA with immunofluorescence staining showing a homogeneous distribution of COL1A1 throughout the dermal layer. Subsequent IHC analysis quantified the increased protein expression, finding a 3.62-fold increase of procollagen type I, a 2.91-fold increase of TGF-β, a 1.54-fold increase of HSP47, and a 1.57-fold increase of tropoelastin in cryolipolysis-treated samples relative to untreated controls. TGF-β is a key element in wound healing and remodeling, known for its ability to stimulate fibroblast proliferation and to increase collagen production. HSP47 is a collagen-specific molecular chaperone which interacts transiently with procollagen during folding, assembly, and transport from the endoplasmic reticulum. Tropoelastin is the soluble precursor to the elastin molecule and is secreted from the cell to form aggregates that become cross-linked and incorporated into elastic fibers.

The significant induction of molecular and protein markers for type I collagen found within the dermis suggests that neocollagenesis may play an essential role in reported skin improvement following cryolipolysis for noninvasive fat reduction. These study results also

demonstrate increased TGF-β and HSP47, indicative of a dermal remodeling process and supportive of TGF-β-fibroblast–mediated neocollagenesis.

The dermal response to nonfreezing cooling treatments can be of importance in areas such as skin rejuvenation, maintenance, and tightening, among others. Moreover, the dual action of skin changes and fat reduction after cryolipolysis could be of great importance in the treatment of complex aesthetic problems, such as cellulite.

CONCLUSIONS

RNA-seq analysis highlighted a gradual upregulation of dermal collagens after treatment. RNA-ISH confirmed upregulation of COL1A1 with a homogeneous spatial distribution. IHC quantification revealed an increase of procollagen type I, TGF-β, HSP47, and tropoelastin. Overall, the data provide the first evidence of dermal remodeling following cryolipolysis and suggest a TGF-β–mediated pathway. This feasibility study is the first to establish the potential mechanism of action behind previously reported clinical observations of skin improvement following cryolipolysis.

Acknowledgments

This clinical study was sponsored by Allergan Aesthetics (Pleasanton, CA), exclusive manufacturer of CoolSculpting. Allergan Aesthetics is an AbbVie (Chicago, Illinois) affiliate.

Disclosures

Dr Stevens is an advisory board member and received research grant support from Allergan Aesthetics (Pleasanton, CA), an AbbVie (Chicago, Illinois) affiliate. Dr Jimenez Lozano and Dr Pham are employees of Allergan Aesthetics, an AbbVie affiliate. Dr Gould declared no potential conflicts of interest with respect to the research, authorship, and publication of this article.

Funding

The authors received no financial support for the research, authorship, and publication of this article.

REFERENCES

1. Manstein D, Laubach H, Watanabe K, Farinelli W, Zurakowski D, Anderson RR. Selective cryolysis: a novel method of non-invasive fat removal. *Lasers Surg Med*. 2008;40(9):595-604.
2. Zelickson B, Egbert BM, Preciado J, et al. Cryolipolysis for noninvasive fat cell destruction: initial results from a pig model. *Dermatol Surg*. 2009;35(10):1462-1470.
3. Avram MM, Harry RS. Cryolipolysis for subcutaneous fat layer reduction. *Lasers Surg Med*. 2009;41(10):703-708.
4. Zelickson BD, Burns AJ, Kilmer SL. Cryolipolysis for safe and effective inner thigh fat reduction. *Lasers Surg Med*. 2015;47(2):120-127.
5. Stevens WG, Bachelor EP. Cryolipolysis conformable-surface applicator for nonsurgical fat reduction in lateral thighs. *Aesthet Surg J*. 2015;35(1):66-71.
6. Stevens WG, Pietrzak LK, Spring MA. Broad overview of a clinical and commercial experience with CoolSculpting. *Aesthet Surg J*. 2013;33(6):835-846.
7. Kilmer SL, Burns AJ, Zelickson BD. Safety and efficacy of cryolipolysis for non-invasive reduction of submental fat. *Lasers Surg Med*. 2016;48(1):3-13.
8. Carruthers JD, Humphrey S, Rivers JK. Cryolipolysis for reduction of arm fat: safety and efficacy of a prototype CoolCup applicator with flat contour. *Dermatol Surg*. 2017;43(7):940-949.
9. Rivers JK, Ulmer M, Vestvik B, Santos S. A customized approach for arm fat reduction using cryolipolysis. *Lasers Surg Med*. 2018;50:732-737. doi.org/10.1002/lsm.22811.
10. Friedmann DP. Cryolipolysis for noninvasive contouring of the periumbilical abdomen with a nonvacuum conformable-surface applicator. *Dermatol Surg*. 2019;45(9):1185-1190.
11. Stevens WG. Does cryolipolysis lead to skin tightening? A first report of cryodermadstringo. *Aesthet Surg J*. 2014;34(6):NP32-NP34.
12. Carruthers J, Stevens WG, Carruthers A, Humphrey S. Cryolipolysis and skin tightening. *Dermatol Surg*. 2014;40 Suppl 12:S184-S189.
13. Bernstein EF, Bloom JD. Safety and efficacy of bilateral submental cryolipolysis with quantified 3-dimensional imaging of fat reduction and skin tightening. *JAMA Facial Plast Surg*. 2017;19(5):350-357.
14. *ZELTIQ Aesthetics FDA 510(K), K172144*, November 1, Silver Spring, MD: U.S. Food and Drug Administration; 2017.
15. Stevens WG. Global perspectives: body contouring in the United States. *ISAPS Newsletter*. 2013;7(3):12-13.
16. Sadick N. Tissue tightening technologies: fact or fiction. *Aesthet Surg J*. 2008;28(2):180-188.
17. Burns JA. Thermage: monopolar radiofrequency. *Aesthet Surg J*. 2005;25(6):638-642.
18. Burns AJ, Dover J, Gregory RO, Zelickson B. Nonsurgical skin tightening modalities. *Aesthet Surg J*. 2007;27(4):423-432.
19. Sasaki GH. Quantification of human abdominal tissue tightening and contraction after component treatments with 1064-nm/1320-nm laser-assisted lipolysis: clinical implications. *Aesthet Surg J*. 2010;30(2):239-245.
20. Oni G, Hoxworth R, Teotia S, Brown S, Kenkel JM. Evaluation of a microfocused ultrasound system for improving skin laxity and tightening in the lower face. *Aesthet Surg J*. 2014;34(7):1099-1110.
21. Sasaki GH, Abelev N, Papadopoulos L. A split face study to determine the significance of adding increased energy and treatment levels at the marionette folds. *Aesthet Surg J*. 2017;37(8):947-960.
22. Araco A. Prospective study on clinical efficacy and safety of a single session of microfocused ultrasound with visualization for collagen regeneration. *Aesthet Surg J*. 2020;40(10):1124-1132.

23. Orringer JS, Kang S, Johnson TM, et al. Connective tissue remodeling induced by carbon dioxide laser resurfacing of photodamaged human skin. *Arch Dermatol*. 2004;140:1326-1332.
24. Orringer JS, Voorhees JJ, Hamilton T, et al. Dermal matrix remodeling after nonablative laser therapy. *J Am Acad Dermatol*. 2005;53:775-782.
25. Hantash BM, Ubeid AA, Chang H, Kafi R, Renton B. Bipolar fractional radiofrequency treatment induces neoelastogenesis and neocollagenesis. *Lasers Surg Med*. 2009;41:1-9.
26. El-Domyati M, El-Ammawi TS, Medhat W, et al. Radiofrequency facial rejuvenation: evidence-based effect. *J Am Acad Dermatol*. 2011;64:524-535.
27. Trapnell C, Roberts A, Goff L, et al. Differential gene and transcript expression analysis of RNA-seq experiments with TopHat and Cufflinks. *Nature protocols*. 2012;7(3):562-578.
28. Gersch RP, Raum JC, Calvert C, Percec I. Fibroblasts derived from human adipose stem cells produce more effective extracellular matrix and migrate faster compared to primary dermal fibroblasts. *Aesthet Surg J*. 2020;40(1):108-117.